# Vertical distribution and radiative effects of mineral dust and biomass burning aerosol over West Africa during DABEX

B. T. Johnson, B. Heese, S. A. Mcfarlane, P. Chazette, A. Jones, N. Bellouin

# Vertical distribution and radiative effects of mineral dust and biomass burning aerosol over West Africa during DABEX

B. T. Johnson,[1] B. Heese,[2] S. A. McFarlane,[3] P. Chazette,[4] A. Jones,[1] and N. Bellouin[1]

Received 22 January 2008; revised 14 May 2008; accepted 4 June 2008; published 12 September 2008.

[1] This paper presents measurements of the vertical distribution of aerosol extinction coefficient over West Africa during the Dust and Biomass-burning Aerosol Experiment (DABEX)/African Monsoon Multidisciplinary Analysis dry season Special Observing Period Zero (AMMA-SOP0). In situ aircraft measurements from the UK FAAM aircraft have been compared with two ground-based lidars (POLIS and ARM MPL) and an airborne lidar on an ultralight aircraft. In general, mineral dust was observed at low altitudes (up to 2 km), and a mixture of biomass burning aerosol and dust was observed at altitudes of 2–5 km. The study exposes difficulties associated with spatial and temporal variability when intercomparing aircraft and ground measurements. Averaging over many profiles provided a better means of assessing consistent errors and biases associated with in situ sampling instruments and retrievals of lidar ratios. Shortwave radiative transfer calculations and a 3-year simulation with the HadGEM2-A climate model show that the radiative effect of biomass burning aerosol was somewhat sensitive to the vertical distribution of aerosol. In particular, when the observed low-level dust layer was included in the model, the absorption of solar radiation by the biomass burning aerosols increased by 10%. We conclude that this absorption enhancement was caused by the dust reflecting solar radiation up into the biomass burning aerosol layer. This result illustrates that the radiative forcing of anthropogenic absorbing aerosol can be sensitive to the presence of natural aerosol species.

**Citation:** Johnson, B. T., B. Heese, S. A. McFarlane, P. Chazette, A. Jones, and N. Bellouin (2008), Vertical distribution and radiative effects of mineral dust and biomass burning aerosol over West Africa during DABEX, *J. Geophys. Res.*, *113*, D00C12, doi:10.1029/2008JD009848.

## 1. Introduction

[2] Aerosols alter the radiative energy budget of the Earth and atmosphere system by scattering and absorbing atmospheric radiation. The impacts on regional and global climate depend on the optical properties of the aerosols and their vertical distribution in the atmosphere. The vertical distribution of absorbing aerosols is especially important as they modify the vertical profile of radiative heating in the atmosphere [e.g., *Quijano et al.*, 2000; *Léon et al.*, 2002; *Won et al.*, 2004; *Ramanathan et al.*, 2007]. This changes the stability of the atmosphere, thereby influencing convective and turbulent motions and clouds [e.g., *Ackerman et al.*, 2000; *Johnson et al.*, 2004; *McFarquhar and Wang*, 2006].

[3] The vertical distribution of aerosol also influences the radiative effect at the top of the atmosphere (TOA), especially when aerosols have strong absorption of shortwave radiation [e.g., *Haywood and Ramaswamy*, 1998; *Meloni et al.*, 2005; *Gadhavi and Jayaraman*, 2006]. For example, the elevation of biomass burning aerosols above marine stratocumulus clouds during the Southern African Regional Science Initiative (SAFARI-2000) greatly enhanced their absorption of shortwave radiation. This led to a positive direct aerosol shortwave radiative effect over the Southern Atlantic, whereas the effect was negative in clear sky conditions [*Keil and Haywood*, 2003; *Abel et al.*, 2005; *Myhre et al.*, 2003a]. *Hsu et al.* [2003] also show the biomass burning aerosols from southeast Asia are frequently lifted into and above cloud and can lead to local reductions of up to 100 W $m^{-2}$ in reflected shortwave irradiance top of the atmosphere via both direct and indirect aerosol effects. The radiative effects of absorbing aerosol in clear skies can also be sensitive to vertical distribution, as shown by *Meloni et al.* [2005], because absorption is enhanced by scattering from aerosols and, to a lesser extent, Rayleigh scattering from below. Recent improvements in the representation of the absorption properties and vertical distribution of biomass burning aerosols in models have contributed to upward revisions in estimates of TOA radiative forcing for biomass burning aerosols [see *Forster et al.*, 2007, section 2.4.4].

[1] Met Office, Exeter, UK.
[2] Leibniz Institute for Tropospheric Research, Leipzig, Germany.
[3] Pacific Northwest National Laboratory, Richland, Washington, USA.
[4] Laboratoire des Sciences du Climat et de l'Environnement, UVSQ, CEA Saclay, CNRS, Gif-sur-Yvette, France.


0148-0227/08/2008JD009848

[4] The vertical distribution of aerosol also has a strong influence on some satellite retrievals. For example, the presence of elevated absorbing aerosol layers can bias satellite retrievals of cloud properties [e.g., *Haywood et al.*, 2004]. Furthermore, the aerosol index retrieved from the Total Ozone Mapping Spectrometer (TOMS) is more sensitive to elevated absorbing layers than layers close to the surface, which can lead to uncertainty in the interpretation of Aerosol Index [e.g., *Ginoux and Torres*, 2003].

[5] During the Dust and Biomass-burning Experiment (DABEX) aerosol vertical distributions were investigated by the Facility for Airborne Atmospheric Measurements (FAAM). The FAAM aircraft included a nephelometer and a Particle Soot Absorption Photometer, which provided an in situ method for deriving aerosol extinction, as a function of altitude. These measurements were coordinated with two ground-based Lidars, and a lidar mounted on a ultralight aircraft as part of the African Monsoon Multidisciplinary Analysis (AMMA) dry season Special Observing Period (SOP0) [*Johnson et al.*, 2007]. These provided frequent measurements of aerosol extinction profile throughout the DABEX campaign. Lidars derive aerosol extinction coefficient from the backscattered signal from a transmitted laser beam. The ratio between extinction and elastic backscatter (the so-called lidar ratio) depends on aerosol size distribution, shape and composition and must be constrained by some additional information. Raman lidar techniques use measurements of Raman backscattering to retrieve the lidar ratio, whereas lidars measuring only elastic backscatter typically use an independent measurement of aerosol optical depth (AOD) to constrain the lidar ratio. In addition, the AERONET Sun photometer at Banizoumbou (50 km from Niamey) provided AODs on most days during DABEX, except those with persistent cloud cover.

[6] Aircraft in situ measurements are typically used to characterize aerosol properties during intensive measurement campaigns, whereas lidars and other remote sensing instruments are relied upon for long-term monitoring and characterization of aerosols. It is therefore important to compare in situ and remote sensing methods to assess whether they lead to consistent estimates of aerosol vertical profile [e.g., *Masonis et al.*, 2002; *Osborne et al.*, 2007; *Schmid et al.*, 2006, and references therein]. This paper compares aerosol extinction profiles made by the three lidars and the FAAM aircraft during AMMA SOP0 (section 3). The influence of aerosol vertical profile on radiative effect is then tested using a single column radiation model (section 4). A climate model simulation with the Met Office Hadley Centre's HadGEM2-A climate model also illustrates the impact of different aerosol layers on radiative effects across the west African region (section 5).

## 2. Methods

### 2.1. Selection of Case Studies for Aircraft and Lidar Comparisons

[7] The FAAM aircraft flew 13 research flights between 13 January and 3 February 2006 from Niamey airport, Niger, West Africa (13.48°N, 2.18°E, 224 m above sea level). These included 35 deep profiles from close to ground level to an altitude above all tropospheric aerosol layers. A total of 23 deep profiles were made in the vicinity of Niamey (with mean distance less than 100 km from Niamey airport). A Portable Lidar System (POLIS) was based at Banizoumbou (13.54°N, 2.66°E, 250 m above sea level) approximately 50 km east-northeast from Niamey from 11 to 30 January 2006. It was also operated at Niamey airport from 31 January to 2 February 2006. A Micropulse Lidar (MPL) was operated at Niamey airport for the duration of 2006 as part of the Atmospheric Radiation Measurement (ARM) Mobile Facility (AMF). An Ultralight Aircraft (ULA) also operated a lightweight lidar during DABEX/AMMA-SOP0 and flew in coordination with the FAAM aircraft on several days.

[8] Five case studies were selected from the DABEX/AMMA-SOP0 period to compare these aircraft and lidar measurements for a range of different aerosol profiles. Table 1 gives details of the case studies, including the dates, times, and availability of data. The locations of lidar ground sites and aircraft tracks during selected profiles are shown in Figure 1. The FAAM aircraft typically covered a horizontal distance of 100 km during deep profiles, whereas the ULA covered much shorter distances and much of the flight tracks were directly above Banizoumbou or Niamey and so are difficult to see in Figure 1.

### 2.2. FAAM Aircraft in Situ Measurements

[9] The FAAM aircraft measured aerosol scattering at 450, 550 and 700 nm, using a three-channel TSI nephelometer and measured aerosol absorption at 567 nm using a Particle Soot Absorption Photometer (PSAP). The sum of scattering and absorption from these instruments provided the aerosol extinction coefficient. Uncertainties came mainly from the angular truncation correction to the nephelometer [*Anderson and Ogren*, 1998]. This correction accounts for the fact that scattering is not detected at angles less than 7° or greater than 170° in the nephelometer. The angular truncation correction is more important, and more uncertain, for dust aerosol since the forward scattering peak is stronger with larger particles. An additional source of error arises from possible losses of large particles within the Rosemount inlet that serves the nephelometer and PSAP. A previous study by *Haywood et al.* [2003a] suggested that particles of radii greater than 1.5 $\mu$m may not be sampled efficiently by the Rosemount inlet. However, applying a correction factor based on the Haywood et al. result led to an overestimation of aircraft-derived AODs in comparisons against AERONET [*Osborne et al.*, 2008]. Therefore, the particle loss correction has been omitted in this study but is acknowledged as a significant source of uncertainty for the extinction coefficient in dust aerosol layers.

[10] The scattering and absorption data were also extrapolated in wavelength to allow comparison with the lidars that operated at 355 nm and 523 nm. The interpolation of scattering coefficient used the Ångström exponent derived from the 450 nm and 550 nm channels of the nephelometer. The variation of absorption coefficient with wavelength was estimated from Mie calculations based on aircraft measurements of size distributions and the refractive indices based on mixtures of dust, black carbon and organic carbon from *World Climate Program* (*WCP*) [1986] (see *Johnson et al.* [2008] and *Osborne et al.* [2008] for details). The method for estimating the relative proportions of biomass burning

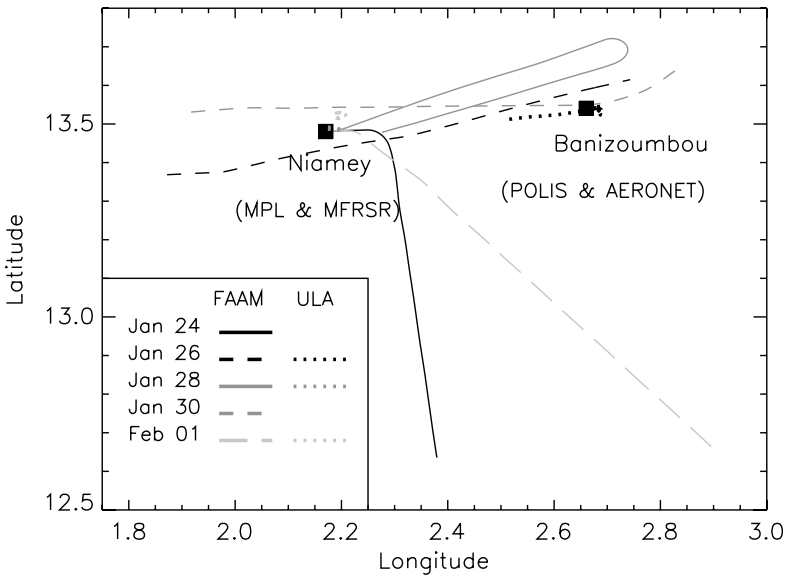


**Figure 1.** Locations of ground-based instruments at Niamey airport and Banizoumbou, plus locations of FAAM (solid and dashed lines) and ULA (dotted lines) aircraft profiles used in the case studies.

aerosol and dust is given in section 4.1.1. The overall uncertainty in the extinction coefficient, resulting from all sources of error above, is estimated to be around ±10% for biomass burning aerosols and ±25% for dust aerosol. Aircraft altitudes were measured by a global positioning system.

### 2.3. POLIS Lidar

[11] The Portable Lidar System (POLIS) is a small, rugged, two channel lidar developed at the University of Munich for easy operation in the field. The compact, frequency doubled and tripled Nd:YAG laser emits pulses at the wavelength of 355 nm, with a repetition frequency of 20 Hz. The data acquisition allows a vertical sampling of 7.5 m. More technical details of this lidar system are described by *Heese et al.* [2002, 2004].

[12] The lidar can be operated with either a depolarization detection unit or a Raman detection unit. The depolarization unit measures the intensity of backscattered light in the plane parallel and cross-polarized plane of the emitted beam. The ratio of these signals gives the volume depolarization, which indicates particle asphericity. The Raman detection unit measures the elastic backscatter at the laser wavelength of 355 nm and inelastic backscatter at 387 nm corresponding to Raman scattering by nitrogen air molecules ($N_2$). The aerosol extinction coefficient was determined directly from the inelastic signal [*Ansmann et al.*, 1992].

[13] The lidar was operated in depolarization mode on most mornings during DABEX as this enabled discrimination between layers dominated by mineral dust or biomass burning. Raman measurements were made on selected nights because the weak Raman signal is easier to distinguish when solar radiation is absent. The two depolarization signals from daytime operations were added together to give a total signal, which was used to derive the extinction profile using the Bernoulli solution to the lidar equation [*Fernald*, 1984; *Klett*, 1985]. The lidar ratios required were determined from the nighttime Raman measurements. A lidar ratio at 355 nm of 55 ± 5 $Sr^{-1}$ in dust layers, and 75 ± 15 $Sr^{-1}$ in biomass burning aerosol layers was calculated from these Raman measurements [*Heese and Wiegner*, 2008]. These lidar ratios also agreed with the results of *Chazette et al.* [2007]. An uncertainty of 15% is estimated for the extinction coefficient from POLIS. This error is mainly based on signal noise [see *Heese and Wiegner*, 2008].

### 2.4. ULA Lidar

[14] The Lidar Aérosol Ultraviolet Aéroporté (LAUVA) lidar system was operated on board an ultralight aircraft (ULA) during DABEX/AMMA-SOP0. This light and compact lidar system implemented on ULA was developed in France by the Commissariat à l'Energie Atomique (CEA) and the Centre National de la Recherche Scientifique (CNRS) for monitoring aerosol dispersion in the low and middle troposphere. It operates with a Nd:Yag laser at the wavelength of 355 nm with a 20 Hz pulse repetition rate. The resolution along the lidar beam path was 1.5 m. Aerosol extinction profiles were obtained from horizontal shooting measurements during profile ascents and the descents, and from nadir shooting measurements at high altitudes above aerosol layers. The horizontal shooting provided were averaged over a path 0.4 to 1 km ahead of the aircraft. The aerosol extinction coefficient was retrieved by the slope method (equation (1)):

$$\alpha_{a355}(z_f) = \frac{1}{2}\frac{\delta Ln[S(s,z_f)]}{\delta s} - \alpha_m(z_f) \quad (1)$$

**Table 1.** Availability and Timings of Data From FAAM, POLIS, MPL, ULA, and AERONET for Five Selected Case Studies

| | Availability/Time of Data Collection (UTC) | | | | |
|---|---|---|---|---|---|
| Date | FAAM | POLIS | MPL | ULA | AERONET |
| 24 Jan 2006 | 0846–0859 | 0857–0936 | 0900 | N/A | 0902 |
| 26 Jan 2006 | 1024–1037 | 1024–1037 | 1030 | 1130–1207 | 0812 |
| 28 Jan 2006 | 0954–1011 | 0000–0300 | N/A | 0923–0954 | N/A |
| 30 Jan 2006 | 0759–0813 | 0759–0813 | 0815 | N/A | 0811 |
| 1 Feb 2006 | 1105–1120 | N/A | 1115 | 0848–0911 | 1118 |

**Table 2.** AOD at 355 nm Estimated From the AERONET Sun Photometer at Banizoumbou, the FAAM Aircraft, and the POLIS Lidar at Banizoumbou on 5 Days During DABEX

| Date | AERONET | FAAM | POLIS |
|---|---|---|---|
| 24 Jan 2006 | 0.45 ± 0.03 | 0.43 ± 0.08 | 0.49 ± 0.1 |
| 26 Jan 2006 | 0.74 ± 0.03 | 0.66 ± 0.15 | 0.53 ± 0.11 |
| 28 Jan 2006 | N/A | 0.45 ± 0.10 | 0.50 ± 0.1 |
| 30 Jan 2006 | 0.80 ± 0.03 | 0.73 ± 0.16 | 0.73 ± 0.15 |
| 1 Feb 2006 | 0.48 ± 0.03 | 0.47 ± 0.10 | N/A |

[15] Here, $\alpha_{a355}(z_f)$ is the aerosol extinction coefficient at 355 nm wavelength, at flight altitude ($z_f$). $S(s, z_f)$ is the range-corrected signal, $s$ is the distance along the lidar beam path and $\alpha_m(z_f)$ is the molecular extinction coefficient at 355 nm wavelength. The relative uncertainty of the ULA lidar-derived lidar ratio was about 25% mainly because of signal noise [*Chazette et al.*, 2007]. Further descriptions of this instrument, its calibration, and data retrieval procedures can be found in the work of *Chazette et al.* [2007].

### 2.5. ARM MPL Lidar

[16] A Micropulse Lidar (MPL) and Multifilter Rotating Shadowband Radiometer (MFRSR) were deployed at Niamey airport from January through December 2006, as part of the Atmospheric Radiation Measurement program's Mobile Facility (AMF) [*Miller and Slingo*, 2007]. The MPL is a 523 nm autonomous lidar system [*Campbell et al.*, 2002]. The measured backscatter profile was corrected for dead time, after-pulse, background signal, and overlap using standard methods [*Campbell et al.*, 2002]. The MPL backscatter profiles were averaged over 15 minute periods to improve the signal to noise ratio. An estimate of AOD was then required to constrain the derived extinction profiles and hence derive the lidar ratio. AODs were retrieved from the MFRSR, which measures total and diffuse solar irradiance at six wavelengths (415, 500, 615, 673, 870, 940 nm). Direct solar irradiance was obtained by differencing the total and diffuse measurements. Spectral values of AOD were then obtained via a Langley regression [*Harrison and Michalsky*, 1994]. The MFRSR AODs were interpolated to 523 nm using the Ångström exponent calculated from AODs at 415 and 870 nm and used to constrain the MPL extinction profiles.

[17] Detailed analysis of MFRSR AODs at a midlatitude site indicate that errors due to calibration are typically <0.01 and errors due to other instrument factors such as instrument tilt, angular response, and filter degradation are also generally <0.01 [*Alexandrov et al.*, 2007]. Previous comparisons at the same site have found agreement within 0.015 root-mean-square error between the MFRSR and other instruments, including an AERONET Sun photometer [*Schmid et al.*, 1999]. The MFRSR uses a shadow band to block the Sun for the diffuse sky measurement, and estimates the solar aureole contribution to the blocked measurement by taking two sideband measurements.

[18] For most aerosol conditions, errors in AOD due to the underestimate of the solar aureole contribution are negligible, however they become more significant for aerosol effective radius >1 $\mu$m because of the larger forward scattering contributions [*Alexandrov et al.*, 2007]. Comparisons to a colocated Sun photometer at Niamey during the latter half of 2006 indicate that the MFRSR underestimates AOD by 15–20%, because of forward scattering by the large dust particles. A correction for the effect of large particle scattering on the MFRSR retrievals at Niamey, following the work of *Russell et al.* [2004], is under development (C. Flynn, personal communication, 2008). For now, an uncertainty of ±20% is assumed for the MFRSR AODs.

[19] For noncloudy periods, vertical profiles of aerosol extinction was retrieved by guessing an initial value of the lidar ratio, solving for the backscatter and extinction at each height [*Fernald*, 1984], and iterating the lidar ratio until the total optical depth calculated from the lidar extinction profile matched the AOD value derived from the MFRSR measurements [*Welton et al.*, 2000]. For cloudy periods the lidar ratio was interpolated between the clearest periods in the data (several per month). Cloudy periods were identified in the MPL data using a cloud detection algorithm based on the method of *Pal et al.* [1992].

### 2.6. AERONET Sun Photometer

[20] The Banizoumbou AERONET Sun photometer was used to measure AODs for the case studies. We used version 2 level 2.0 direct Sun AODs at 438 and 675 nm (obtained from http://aeronet.gsfc.nasa.gov). Measurement times were picked to coincide with the times of the FAAM profiles (Table 1). Interpolation was used to estimate the AODs at 355 nm and 523 nm for comparison with the lidars. The interpolation assumed a constant Ångström exponent, which was obtained from the difference in AOD between 438 nm and 675 nm. We expect the interpolation to introduce a small error of up to 2% in the 355 nm AOD, due to the wavelength dependence of Ångström exponent. On 28 January thin cloud prevented accurate measurements by AERONET so no AOD data was available. An uncertainty of ±0.03 is assumed for AODs on the basis of calibration and wavelength interpolation errors.

## 3. Results of Lidar and Aircraft Comparison

### 3.1. Comparison of AODs Against AERONET

[21] Because the lidar and aircraft in situ measurements have uncertainties associated with aerosol physical and optical properties, it was important to evaluate them against an independent and more reliable measurement of the aerosol column. Tables 2 and 3 compare AODs integrated from the FAAM, POLIS and MPL extinction profiles against AODs interpolated from AERONET data (see section 2.6). Since the Sun photometer does not rely on assumptions regarding aerosol properties it was considered to be the most accurate measurement of AOD in this comparison. The POLIS AODs are estimated from the daytime extinction profiles using campaign mean lidar ratios derived from the nighttime Raman measurements;

**Table 3.** AOD at 523 nm Estimated From the AERONET Sun Photometer at Banizoumbou, the FAAM Aircraft, and the MFRSR at the ARM Mobile Facility, Niamey Airport, on 5 Days During DABEX

| Date | AERONET | FAAM | MPL (MFRSR) |
|---|---|---|---|
| 24 Jan 2006 | 0.31 ± 0.03 | 0.37 ± 0.07 | 0.29 ± 0.06 |
| 26 Jan 2006 | 0.64 ± 0.03 | 0.65 ± 0.14 | 0.49 ± 0.10 |
| 28 Jan 2006 | N/A | 0.44 ± 0.10 | 0.55 ± 0.11 |
| 30 Jan 2006 | 0.67 ± 0.03 | 0.71 ± 0.16 | 0.60 ± 0.12 |
| 1 Feb 2006 | 0.40 ± 0.03 | 0.46 ± 0.10 | 0.38 ± 0.08 |

75 $Sr^{-1}$ for biomass burning aerosol and 55 $Sr^{-1}$ for dust, as derived by *Heese and Wiegner* [2008].

[22] The FAAM aircraft underestimated AOD at 355 nm by an average of 7% and overestimated AOD at 523 nm by an average of 8%, compared to AERONET, over the four available comparison days. These differences are smaller than the uncertainties in the FAAM AOD (10–25%, see section 2.2), indicating a reasonable agreement within the uncertainty range. The comparison at 355 nm may not be as reliable since it is outside the range of nephelometer and AERONET wavelengths. Column mean Ångström exponents from the nephelometer, used in the interpolation, were around 0.2 lower than those given by AERONET, which would have given a 5% low bias to the FAAM AOD at 355 nm. Errors in the nephelometer-derived AOD may be caused by uncertainties in the angular truncation corrections given by *Anderson and Ogren* [1998]. These corrections are wavelength-dependent and become more uncertain in dusty conditions because large and aspherical particles have more irregular scattering phase functions. Additional uncertainty arises from possible losses of coarse particles during aircraft sampling with Rosemount inlets. However, correcting for anticipated losses led to an overestimation of AOD by up to 30% at 550 nm, as shown by further comparisons by *Osborne et al.* [2008]. Past comparisons of airborne nephelometers against Sun photometers have shown good agreement or underestimation by the nephelometer [e.g., *Haywood et al.*, 2003b; *Osborne et al.*, 2007; *Schmid et al.*, 2006, and references therein].

[23] POLIS AODs were within 25% of AERONET AODs at 355 nm on individual days, and the mean AOD from POLIS was just 9% lower than the mean AERONET AOD. This indicates that POLIS performed reasonably well in deriving the absolute magnitude of aerosol extinction, given the uncertainty range of 15% associated with POLIS AODs (see section 2.3). The comparison was however limited to just 3 days (24, 26 and 30 January) since POLIS data was not available on 1 February. The POLIS AOD was 20% higher than the AERONET AOD on 24 January, probably because of extrapolation of unrepresentative high extinction values at 500 m to the ground, as shown in Figure 2.

[24] The MFRSR AODs were within 10–20% of AERONET AODs on the 4 days that data were available. The average AOD from MFRSR was just 6% lower than that from AERONET. Such differences may have been due to the geographic distance (55 km) between Banizoumbou and Niamey, different measurement times and potential underestimate of MFRSR AOD during large particle conditions (see section 2.5). However, the differences are well within the 20% uncertainty suggested in section 2.5. On 26 and 28 January, midlevel and high-level clouds made MFRSR retrievals difficult and AODs were interpolated from surrounding cloud-free days. ULA AODs were not assessed in this study.

[25] The comparisons on 26 and 28 January may be affected by temporal variability of the AOD since some measurement times differ by 2 h or more (see Table 1). Time series of AERONET observations showed a variability of 0.1 in AODs (at 440 nm) during the days (0700–1700 UTC) of our comparison study. This will lead to additional uncertainty for comparisons where timings were not coincident.

### 3.2. Comparison of Aerosol Extinction Profiles

[26] Figure 2 compares profiles of aerosol extinction at 355 nm from the FAAM aircraft, POLIS lidar and ULA lidar. Figure 3 compares profiles of aerosol extinction from the MPL lidar and FAAM aircraft at 523 nm. The FAAM mean profiles (Figures 2f and 3e) were calculated including 23 FAAM aircraft profiles taken between 13 January and 3 February, all with a mean distance of less than 100 km from Niamey. The POLIS mean profile included 2–3 h of data taken each morning on 20 days between 11 January to 2 February, and the MPL mean profile included 3.5 h of MPL lidar data taken from 0800 to 1130 UTC on 19 days from 13 January to 3 February. The FAAM profiles in Figures 2 and 3 are slightly different as the data was interpolated to different wavelengths.

[27] The vertical structure of aerosol extinction varied quite widely during DABEX, as illustrated by the selected case studies. However, in general the aerosol extinction was highest in the lowest 1 km of the atmosphere. This was caused by high loadings of dust aerosol in the local boundary layer, as shown in section 4.1.1. Aerosol extinction generally decreased with height and typically fell to negligible value between 4 and 5 km. On 24 January and 1 February there were peaks in extinction between 2 and 5 km associated with thick layers of biomass burning aerosol whereas on other days the elevated biomass burning aerosol layers were not so prominent.

[28] The aircraft in situ measurements and lidar data agreed reasonably well on the relative magnitude and vertical gradient of aerosol extinction. Details such as the height of distinctive layers were also reasonably consistent between the FAAM in situ measurements and lidar profiles, though not in all cases. Differences in the height of layers, and the exact shape of extinction profiles may have been partly caused by differences in the timing and location of profiles (see Figure 1 and Table 1). Similar differences have been seen in previous intercomparisons of lidar against aircraft in situ measurements and have also been attributed to spatial or temporal differences in sampling in inhomogeneous aerosol fields [*Osborne et al.*, 2007; *Schmid et al.*, 2006].

[29] The ULA extinction is slightly lower than POLIS or FAAM in the lowest 1.5 km and slightly greater at higher altitudes but the discrepancies are generally small and within the error bars of each instrument. The uncertainties in FAAM extinction varied from 10 to 25% and increased with the proportion of dust (see section 2.2) so were generally greater at lower altitudes. The uncertainty range of the ULA lidar was ±25%, mainly because of signal noise. Uncertainties in the aerosol extinction from the ULA lidar may also arise from temporal and spatial variability of the aerosol microphysical properties and their extinction-to-backscatter ratio (lidar ratio). The vertical profile of lidar ratio used by the ULA was determined from nadir-shooting profiles close to the beginning of descents, or the end of ascents.

[30] The POLIS and FAAM extinction profiles followed each other quite closely and generally agreed, within the uncertainty ranges. The uncertainty in POLIS extinction was estimated to be around 15% mainly because of signal noise, which causes difficulty in determining the lidar ratio (see section 2.4). The POLIS lidar tended to give higher values of extinction below 1 km, although this is not true on the 26 January case. These deviations may have been partly

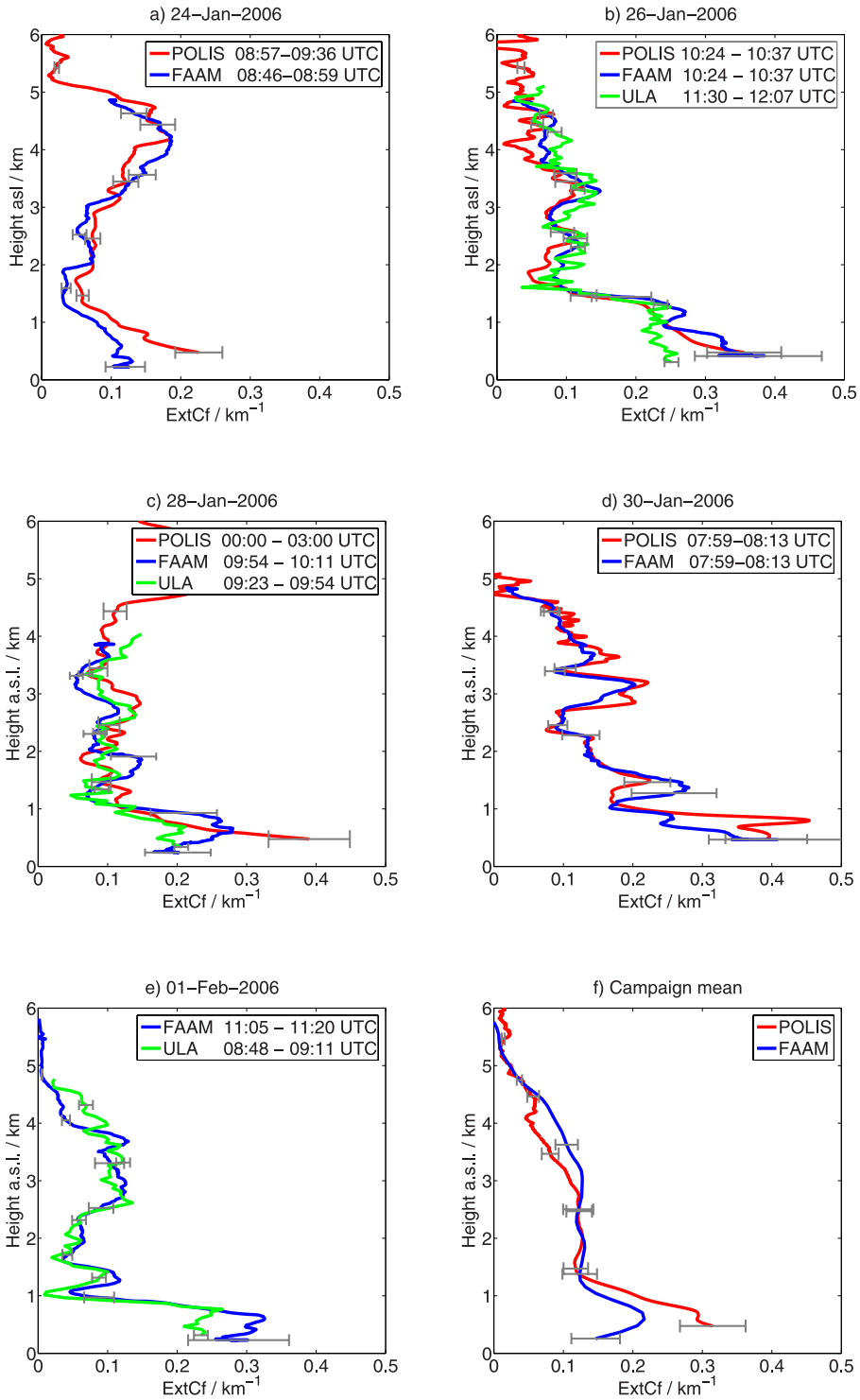


**Figure 2.** Aerosol extinction (at 355 nm) as a function of height above sea level from the POLIS lidar, FAAM aircraft, and ULA lidar on 5 days during DABEX, plus a campaign mean averaged over all available profiles from DABEX.

due to variability of aerosol within the boundary layer. For example, the POLIS profile for 28 January (Figure 2c) indicates a lower boundary layer top, which might be expected since it was taken at nighttime. There is also slightly lower extinction by POLIS in the mean profile at 3–4.5 km. These may be partly due to data sampling, since POLIS and FAAM data had different patterns of availability through the averaging period. In the biomass burning layer an underestimation of the lidar ratio may cause a slight overestimation of extinction.

[31] The MPL extinction profiles did not follow the FAAM profiles as closely, compared to the POLIS comparisons. In the case studies the MPL was often much lower than FAAM in the lower aerosol layers (below 2 km). In some places these

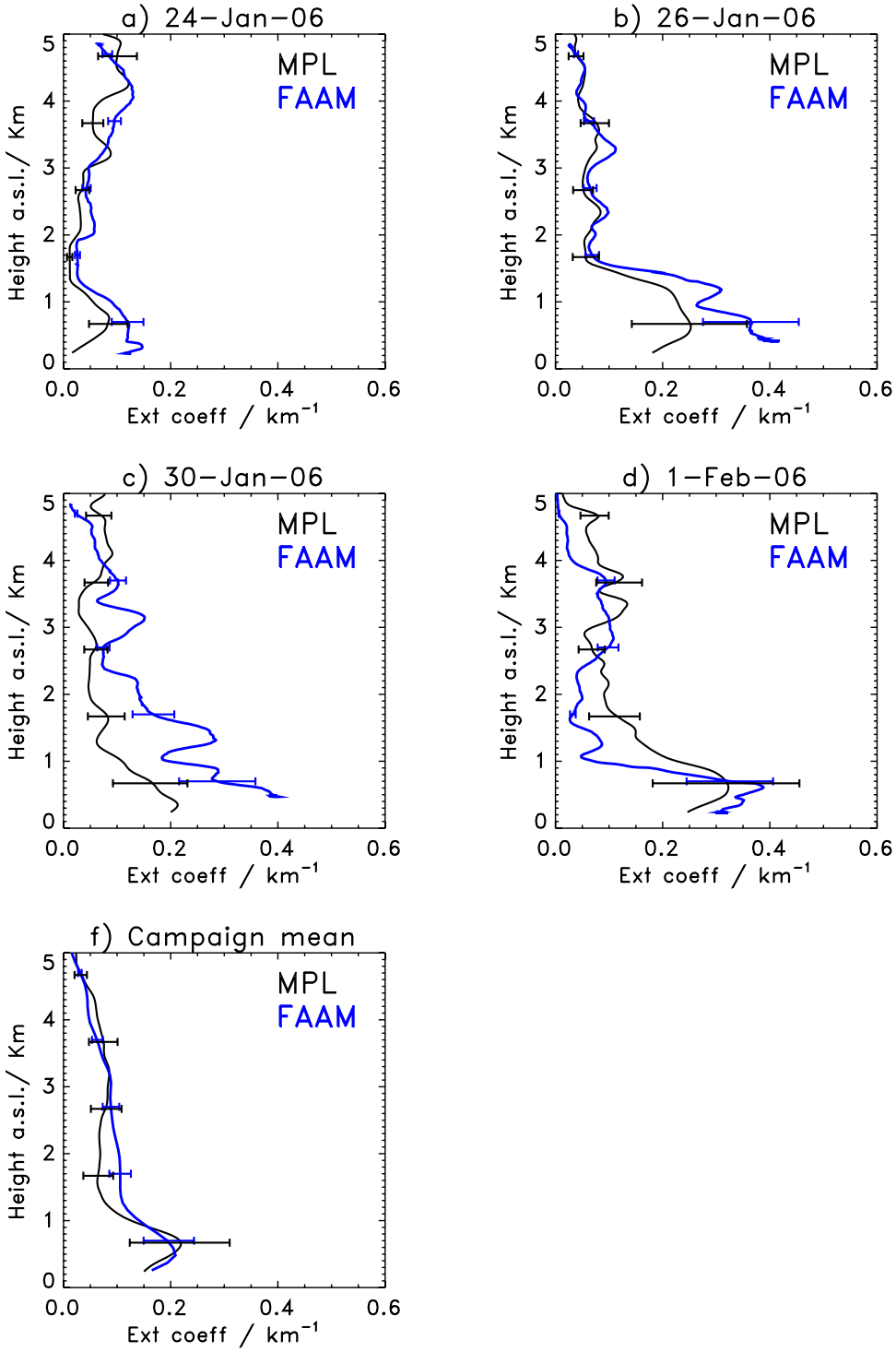


**Figure 3.** Aerosol extinction (at 523 nm) as a function of height above sea level from the FAAM aircraft and ARM MPL lidar on 5 days during DABEX.

differences were outside the uncertainty ranges. In the upper layers (above 2 km) the extinction was in better agreement. This disagreement in the vertical gradient of extinction is unlikely to be caused by the assumption of a constant lidar ratio with height. Estimates of the lidar ratio at 523 nm, performed as part of this study, suggest that the constant lidar ratio assumption would lead to a 6% underestimation for dust aerosol and an 18% overestimation for biomass burning aerosol. Interestingly, no discrepancy occurs in the mean profile below 2 km. This shows that the discrepancies are rather case-dependent and may be related to local variations in aerosol on the comparison days.

[32] Uncertainty in the MPL profiles close to the surface, may also be caused by uncertainty in the lidar overlap correction. The overlap function is a multiplicative factor that corrects for loss of signal due to poor optical efficiency of the telescope in the near range of the lidar. For the Niamey MPL, the overlap correction is significant (>3%) to

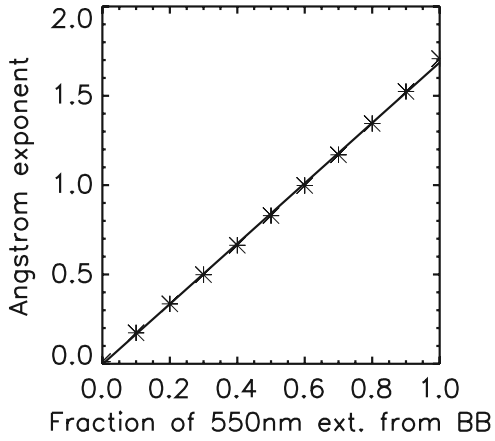


**Figure 4.** Relationship between the Ångström exponent and the fraction of extinction at 550 nm associated with biomass burning (BB) aerosol rather than dust. Mie calculations are shown in asterisks, and a linear regression fit is shown as a solid line.

a distance of about 3.5 km. The exact uncertainty in the overlap function used for the Niamey MPL is not available; error analysis by *Welton and Campbell* [2002] indicates that uncertainty in the overlap correction is typically on the order of 5–10% of the overlap function itself. On the basis of the uncertainty in MFRSR AODs used to constrain the MPL profiles (20%), the assumption of constant lidar ratio in the retrieval (18% in biomass burning layer; 6% in dust layer), and the assumed overlap uncertainty (±10% below 2 km; ±5% below 4 km), the total uncertainty in the retrieved extinction profiles from the MPL was estimated to be 36% below 2 km and 43% above 2 km.

## 4. Single-Column Calculations of Aerosol Radiative Effects

[33] As discussed in section 1, the vertical distribution of aerosol extinction can have an important influence on aerosol radiative effects. Since we have reasonable confidence in the vertical profile of aerosol extinction from the FAAM aircraft, based on the comparisons above, the FAAM aircraft data has been used as to provide inputs for a single-column radiative transfer model. The sensitivity of radiative effects to the vertical distribution of aerosol extinction has been investigated using observed and idealized profiles of aerosol extinction.

### 4.1. Radiative Transfer Model Setup

[34] The Edwards and Slingo radiative transfer model [*Edwards and Slingo*, 1996] was used to calculate shortwave radiative fluxes for single atmospheric columns representing the mean conditions observed over Niamey during DABEX. The model used 220 spectral bands covering wavelengths from 0.2 to 10 $\mu$m and used the two stream Delta-Eddington approximation. Solar parameters were set up for 15 January and a latitude of 13.5N to resemble January mean conditions at Niamey. Diurnal mean radiative fluxes were calculated by averaging fluxes over a single daily cycle of solar zenith angles. Direct radiative effects were calculated as the change in net shortwave flux at either the TOA, the surface (SFC), or across the atmosphere (ATM), as a result of including a particular aerosol species. In most calculations the background atmospheric state was assumed to be aerosol free, although in one case biomass burning radiative effects were calculated assuming that mineral dust aerosol was part of the background atmospheric state. All calculations assumed cloud-free conditions.

#### 4.1.1. Vertical Profiles of Aerosols and Atmospheric Constituents

[35] Profiles of aerosol extinction, humidity, ozone concentration and temperature were calculated by averaging together all FAAM aircraft profiles from DABEX made within 100 km (mean distance) of Niamey. This included 23 profiles from 12 flights. Where more than one profile was available per day an average was calculated for that day first, then the campaign mean was calculated giving each day an equal weighting. The averaged profile data extended from the surface to an altitude of 5 km above mean sea level. Above 5 km, temperature, humidity and ozone profiles were specified from the standard tropical atmosphere profiles of *McClatchey et al.* [1972] and aerosol extinction was assumed to be zero.

[36] For the modeling work it was essential to have an estimate of which aerosol species contributed most to aerosol extinction at different altitudes. Analysis of filter samples confirmed that mineral dust and biomass burning aerosol were the dominant sources of aerosols during DABEX/AMMA SOP0 [*Formenti et al.*, 2008; *Rajot et al.*, 2008]. Chemical transport model simulations also showed that biomass burning emissions dominated the fine particle AOD over West Africa with only a small contribution from fossil fuel and biofuel combustion and secondary organic aerosol production (G. Myhre et al., Modeling of the solar radiative impact of biomass burning aerosols during the DABEX experiment, submitted to *Journal of Geophysical Research*, 2008). We therefore refer to the fine aerosol mode in our simulations as the biomass burning component. Our model simulations also include a representation for the dust aerosol.

[37] The Ångström exponent measured by the nephelometer provided a good indication as to the relative proportions of dust and biomass burning aerosol in the observations [see *Johnson et al.*, 2008, Figure 5]. Ångström exponents were measured by the FAAM aircraft nephelometer using the 450 nm and 700 nm channels. Value ranged from 0 to $-0.2 \pm 0.1$ in pure dust layers [*Osborne et al.*, 2008] to $1.5 \pm 0.1$ in layers dominated by aged biomass burning aerosol layers [*Johnson et al.*, 2008]. Mie calculations based on lognormal fits to the Passive Cavity Aerosol Spectrometer Probe (PCASP) data and assumed refractive indices gave Ångström exponents of 0.01 for dust aerosol and 1.7 for aged biomass burning aerosol. Differences between nephelometer and Mie-calculated Ångström exponents were attributed to difficulties in accounting for coarse particles above 1.5 $\mu$m in radius. The uncertainty in nephelometer derived Ångström exponent (±0.1) stems from uncertainty in the wavelength dependence of the nephelometer corrections (see section 2.2). The Mie-derived aerosol optical properties from the Johnson et al. and Osborne et al. studies were combined to examine the relationship between Ångström exponent and the relative contributions of dust and biomass burning aerosol to aerosol extinction. The results show a nearly linear relationship (Figure 4) between the Ångström

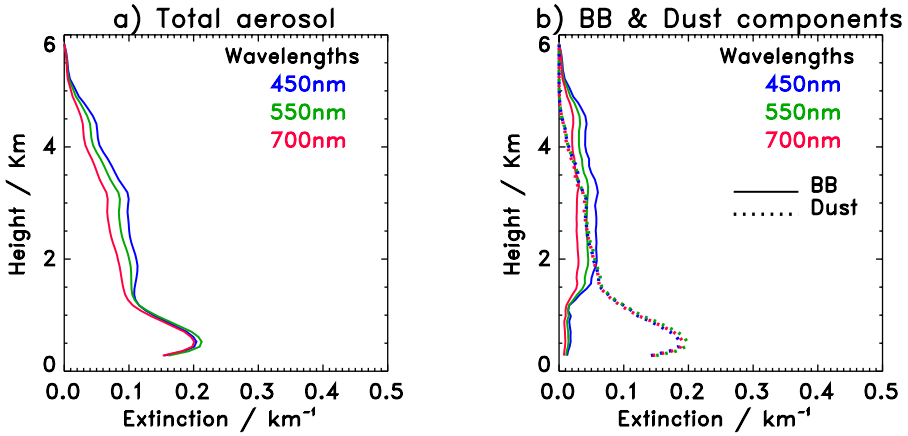


**Figure 5.** DABEX campaign mean profiles of aerosol extinction at 450 nm, 550 nm, and 700 nm, including (a) total aerosol extinction and (b) biomass burning (BB) aerosol component (solid lines) and mineral dust component (dotted line), as a function of height above sea level (km).

exponent and the fraction of extinction attributable to biomass burning aerosol. Therefore, linear regression was used to determine the proportion of aerosol extinction associated with dust and biomass burning aerosol extinction from the nephelometer Ångström exponent, as shown in Figure 4. The instrumental uncertainty in Ångström exponent (±0.1) would lead to potential errors of about 6% in the fraction of dust or biomass burning aerosol extinction to total aerosol extinction.

[38] The resulting extinction profiles for total aerosol and the dust and biomass burning aerosol components are shown in Figure 5 for wavelengths of 450 nm, 550 nm and 700 nm. The dust component peaks near the surface (1 km), whereas the biomass aerosol component peaks around 2–3 km. These extinction profiles correspond to an AOD of 0.29 for the dust component, and an AOD of 0.16 for the biomass burning aerosol component (at 550 nm). These AOD estimates should be treated cautiously since they will be influenced by wavelength-dependent errors in nephelometer corrections, errors due to the nonspherical shape of dust particles, and inaccuracies within the size distributions and refractive indices assumed for the Mie calculations.

[39] Idealized profiles of aerosol extinction were also used for a sensitivity experiment. These had uniform aerosol concentrations within two prescribed layers. The altitude of lower layer ranged from the surface (250 m above mean sea level) to 2.5 km, and the altitude of the upper layer ranged from 2.5 to 5 km. In the first experiment dust was put in the lower layer and biomass burning aerosol was put in the upper layer. In a second experiment the arrangement was reversed so that the dust was above, and the biomass burning aerosol was below. The optical depth for each aerosol species was the same as used in the nonidealized experiments.

[40] Aerosol single scattering albedos and asymmetry parameters were calculated from Mie calculations based on typical size distributions from the FAAM aircraft PCASP instrument, as presented by *Johnson et al.* [2008] and *Osborne et al.* [2008]. The refractive index for dust was given by *WCP* [1986] but with the imaginary part of the refractive index for dust scaled down by a factor of 10 to give agreement between the calculated single scattering albedo at 550 nm and the single scattering albedo observed via the FAAM nephelometer and PSAP on two flights sampling dust aerosol [*Osborne et al.*, 2008]. The biomass burning aerosol refractive index was estimated by representing the aerosol as an internal mixture of black carbon and nonabsorbing organics with refractive index for each component from *WCP* [1986]. The proportion of black carbon was assumed to be 12.5% by mass as this gave agreement between the calculated single scattering albedo and the observed mean value from 7 flights where the aerosol was dominated by aged biomass burning aerosol [*Johnson et al.*, 2008]. The biomass burning aerosol had a fairly low single scattering albedo of 0.81 ± 0.05 at 550 nm, whereas the dust had a high single scattering albedo of 0.98 ± 0.02 at 550 nm. The uncertainty estimates on these values indicate instrumental error and uncertainty owing to variability in the observations. Assuming dust to be spherical particles (assumed in the Mie calculations) may introduce small errors in optical properties and radiative effects. *Osborne et al.* [2008] compare optical properties from Mie theory against optical properties from T-matrix calculations for a variety of aerosol shapes (columns, plates, spheroids). Their overall conclusion was that nonsphericity can introduce errors of up to 21% for extinction coefficients derived from the FAAM data during DABEX.

#### 4.1.2. Representation of Surface Albedo

[41] The land surface albedo was specified as a function of wavelength based on radiometer measurements of upwelling and downwelling radiation during aircraft runs 500 ft (150 m) above the ground in the Niamey region. This gave a broadband (solar-weighted average) albedo of 0.28 but the albedo increased strongly with wavelength, as expected for a visually orange/brown surface. To explore the sensitivity of results to surface albedo, calculations were also made using ocean surface albedos. These were calculated as a function of wavelength and solar zenith angle from *Cox and Munk* [1954] and were typically in the range 0.02–0.07 across the solar spectrum.

### 4.2. Aerosol Radiative Effects

[42] All results of single-column calculations are given in Table 4. The uncertainty in these estimates comes mainly from the uncertainty in the aircraft derived extinction, which is estimated to be about 20%. Dust and biomass burning aerosol both depleted the net solar radiation at the surface

**Table 4.** Direct Shortwave Aerosol Radiative Effects at the Surface, Across the Atmosphere, and at the Top of the Atmosphere Over Land and Ocean Surfaces and for DABEX Campaign Mean Profiles and Idealized Profiles[a]

| | Radiative Effects (W m$^{-2}$) | | | | | |
|---|---|---|---|---|---|---|
| | Land | | | Ocean | | |
| | SFC | ATM | TOA | SFC | ATM | TOA |
| Mean profiles | | | | | | |
| Dust and BB | −21.8 | 15.0 | −6.8 | −31.5 | 13.4 | −18.0 |
| Dust only | −12.8 | 5.7 | −7.1 | −19.9 | 5.2 | −14.6 |
| BB only | −10.7 | 9.5 | −1.2 | −14.1 | 8.3 | −5.8 |
| BB only (background dust included) | −9.0 | 9.3 | 0.3 | −11.6 | 8.2 | −3.4 |
| Idealized profiles | | | | | | |
| BB above dust below | −21.9 | 15.3 | −6.6 | −31.5 | 13.7 | −17.8 |
| BB below dust above | −22.0 | 13.6 | −8.4 | −31.4 | 11.8 | −19.6 |

[a]Abbreviations are as follows: SFC, at the surface; ATM, across the atmosphere, TOA, top of the atmosphere.

(SFC) because of a combination of backscattering and absorption of downwelling solar radiation. The surface effect was higher for the dust than the biomass burning aerosol (−12.8 W m$^{-2}$ for dust, and −10.7 W m$^{-2}$ for biomass burning aerosol) because of its higher contribution to AOD (0.29 for dust and 0.16 for biomass burning aerosol, at 550 nm wavelength). However, the increase in atmospheric absorption (ATM) was greater for the biomass burning aerosol (9.5 W m$^{-2}$) than for the dust (5.7 W m$^{-2}$) because of the lower single scattering albedo of the biomass burning aerosol (see above). Note, the ATM effect includes changes in the amount of absorption by gases such as water vapor, due to aerosols modifying the intensity of upwelling and downwelling radiative fluxes.

[43] The biomass burning aerosol TOA radiative effect was close to zero (−1.2 W m$^{-2}$), because the effects of backscattering and absorption approximately cancel. This result is sensitive mainly to the single scattering albedo of the biomass burning aerosol; the instrumental uncertainty of 0.05 in single scattering albedos at 550 nm leads to a uncertainty of 1.9 W m$^{-2}$ in the TOA radiative effect. The TOA radiative effect for biomass burning aerosol is consistent with the close to neutral clear-sky TOA radiative effect found by Myhre et al. (submitted manuscript, 2008) over the border regions between the Sahel and Sahara desert. Much lower (more negative) radiative effects have been found for biomass burning aerosols in the past. For example, *Abel et al.* [2005] and *Myhre et al.* [2003a] found clear-sky TOA radiative effects of −7.6 to −9.1 W m$^{-2}$ and −3 to −5 W m$^{-2}$ over broad regions centered on Southern African region, based on observations from SAFARI-2000. *Ross and Hobbs* [1998] found TOA radiative effects of −20 W m$^{-2}$ over forest and −8 W m$^{-2}$ over cerrado (grass and small bushes) per AOD, based on measurements from the Smoke Clouds and Radiation Brazil (SCAR-B). The higher (closer to zero) TOA radiative effect found during DABEX can be explained partly by the moderate to high surface albedo (broadband value of approximately 0.28) and the lower single scattering albedo of the biomass burning aerosol compared to measurements in Southern Africa and South America [see *Johnson et al.*, 2008, section 6].

[44] The biomass burning aerosol also reduced the net radiative flux at the surface by 10.7 W m$^{-2}$, whilst 9.5 W m$^{-2}$ more energy was absorbed in the atmosphere. This redistribution of energy would stabilize the troposphere and reduce surface evaporation, thereby slowing down the hydrological cycle. Radiative heating in the free troposphere may also lead to responses in large-scale atmospheric circulations. Exploring these more far-reaching influences of the aerosol is beyond the scope of this study.

[45] The TOA radiative effect for dust was strongly negative at −7.1 W m$^{-2}$ and so was the effect on surface radiation (−12.8 W m$^{-2}$). The absorption of shortwave radiation in the atmosphere increased by 5.7 W m$^{-2}$ because of the dust, although it should be noted that this may come partly through enhancing gaseous absorption since the dust itself was not strongly absorbing, having a single scattering albedo of 0.98 at 550 nm. The longwave effects of dust were not considered here but may be comparable to the shortwave effects [e.g., *Tanŕe et al.*, 2003; *Myhre et al.*, 2003b]. When dust and biomass burning aerosols were both included together it led to a SFC effect of −21.8 W m$^{-2}$, an ATM effect of 15.0 W m$^{-2}$, and a TOA effect of −6.8 W m$^{-2}$. These estimates are all about a factor of 2 lower than the radiative effects calculated by *Mallet et al.* [2008], which were based on observations made at Djougou (9.8°N, 1.6°E). This difference can be partly explained by the higher AODs and lower single scattering albdeos observed at Djougou, as it was close to the most intense biomass burning regions (Myhre et al., submitted manuscript, 2008).

[46] Radiative forcing efficiencies (radiative effects/AOD) are given in Table 5. Since the biomass burning aerosol is more absorbing than the dust it is more efficient (per unit AOD) at reducing solar radiation at the surface and increasing absorption in the atmosphere. In contrast the dust is more efficient at decreasing the TOA solar flux.

[47] When the ocean surface albedo scheme was used instead of the observed land albedo, the TOA radiative effect for biomass burning aerosols was negative and fairly substantial (−5.8 W m$^{-2}$). The radiative effect on atmospheric absorption (ATM) was also lower over ocean because the reflected (upwelling) solar flux was lower. The surface radiative effect (SFC) was higher over ocean because a larger proportion of the downwelling solar flux is absorbed at the ocean surface, thus amplifying this term. These processes also lead to higher SFC and TOA forcing efficiencies over the ocean but slightly lower ATM forcing efficiency (Table 5).

[48] Whilst these ocean surface calculations were hypothetical experiments the scenario was not unrealistic. Obser-

**Table 5.** Direct Shortwave Aerosol Radiative Forcings Efficiency at the Surface, Across the Atmosphere, and at the Top of the Atmosphere, Over Land and Ocean Surfaces and for DABEX Campaign Mean Profiles[a]

| | Radiative Forcing Efficiency (W m$^{-2}$) | | | | | |
|---|---|---|---|---|---|---|
| | Land | | | Ocean | | |
| | SFC | ATM | TOA | SFC | ATM | TOA |
| Mean profiles | | | | | | |
| Dust and BB | −48.5 | 33.4 | −15.2 | −69.9 | 29.9 | −40.0 |
| Dust only | −43.9 | 19.6 | −24.3 | −68.1 | 17.9 | −50.2 |
| BB only | −68.0 | 60.1 | −7.8 | −88.8 | 52.4 | −36.5 |

[a]Abbreviations are as follows: SFC, at the surface; ATM, across the atmosphere; TOA, top of the atmosphere.

vations made during the Dust Outflow and Deposition over the Ocean (DODO) experiment [*McConnell et al.*, 2008] showed elevated layers of biomass burning aerosols over the Atlantic ocean, 100–200 km off the coast of Guinea. In a similar manner to DABEX, mineral dust aerosol layers were mainly confined to the lowest 1.5 km of the atmosphere [see *Capes et al.*, 2008; *McConnell et al.*, 2008, Figure 5].

[49] The radiative effects of biomass burning aerosol were somewhat sensitive to whether dust was included as part of the background state (row 4 of Table 4). For example, the TOA radiative effect increased from $-1.2$ W m$^{-2}$ to 0.3 W m$^{-2}$ over land and from $-5.8$ W m$^{-2}$ to 3.4 W m$^{-2}$ over ocean when dust was included as part of the background state. The increase occurred because more solar radiation was reflected upward by the dust via backscattering. This increased the upwelling fluxes through the atmosphere, increasing absorption by the biomass burning aerosol. This kind of change, though relatively small, is important since there is still considerable uncertainty as to the sign of the TOA radiative forcing of biomass burning aerosol [*Forster et al.*, 2007]. It is somewhat confusing that the radiative effect on absorption of solar radiation through the atmosphere (ATM) was not changed when dust was included as part of the background state. This may be because the biomass burning aerosol layer decreased the amount of solar radiation absorbed by the dust and atmospheric gases below it.

[50] The experiments with idealized aerosol profiles showed that the radiative effects were somewhat sensitive to how the dust and biomass burning aerosol were distributed in the vertical. For example, swapping the configuration of aerosols so that the biomass burning aerosol was below, and the dust was above (contrary to the observed situation) decreased the TOA radiative effect by 1.8 W m$^{-2}$ over land (a decrease from $-6.6$ to $-8.4$ W m$^{-2}$) and by 1.8 W m$^{-2}$ over ocean (a decrease from $-17.8$ to $-19.6$ W m$^{-2}$), see Table 4. The ATM radiative effect also decreased by 1.7 W m$^{-2}$ over land, and 1.9 W m$^{-2}$ over ocean. This experiment clearly shows that shortwave radiative effects were sensitive to aerosol vertical distribution, although the magnitude of the changes were only of order 10% of the total radiative effect at the surface. A simple explanation is that when the dust layer was beneath the biomass burning aerosol it increased the amount of solar radiation scattered up into the biomass burning aerosol layer. This would have increased the absorption of solar radiation by the biomass burning aerosol. When the dust layer was above the biomass burning aerosol layer it would have shadowed the biomass burning aerosol layer, reducing absorption of solar radiation by the biomass burning aerosol. A more detailed radiative transfer study, such as a Monte Carlo simulation or ray-tracing radiance code, would be required to quantify these processes.

## 5. Climate Model Simulation of Aerosol Radiative Effects Over West Africa

### 5.1. HadGEM Climate Model Simulations

[51] The climate model used was HadGEM2-A, the atmospheric component of the Hadley Centre Global Environment Model version 2, a development of the previous version HadGEM1 [*Johns et al.*, 2006; *Martin et al.*, 2006]. It is a grid point model with a resolution of 1.25° latitude by 1.875° longitude, with 38 levels in the vertical up to about 40 km. The configuration of the model used here includes schemes to interactively simulate biomass burning aerosols as well as three natural aerosol species: sulfate from dimethyl sulfide and volcanic emissions, mineral dust and sea-salt aerosols.

[52] The biomass burning aerosol scheme is based on *Davison et al.* [2004], the sulfate and sea-salt schemes on *Jones et al.* [2001], and the mineral dust scheme on *Woodward* [2001]. These schemes have been much improved for HadGEM2 as detailed by *Bellouin et al.* [2007]. The biomass burning emissions used were those of *Dentener et al.* [2006]. Volcanic sulfur emissions were taken from *Andres and Kasgnoc* [1998], and DMS emissions were calculated interactively on the basis of the concentration of DMS in seawater [*Kettle et al.*, 1999]. The optical properties of mineral dust and biomass burning aerosol were specified using FAAM aircraft data from the DABEX campaign, presented by *Johnson et al.* [2008] and *Osborne et al.* [2008]. The AODs of biomass burning aerosol and dust were also adjusted to match the observed values from aircraft profiles in the Niamey region (see section 4 for details). This was achieved by increasing mass concentration of biomass burning AOD by a factor of 2.4 and increasing mass concentrations of dust optical depth by a factor of 4.4. The radiation scheme is a six-band version of the *Edwards and Slingo* [1996] code treating solar fluxes from 0.2 to 10 $\mu$m.

[53] The HadGEM model was run for 3 years with present day emissions of biomass burning and natural aerosols (dust, sea salt, and sulphate from volcanic and DMS emissions). This was compared against a 3-year run with only natural aerosols, and a run with only biomass burning aerosols. Although these were global runs, the analysis below focuses on January mean fields over northwest Africa to enable comparison with DABEX/AMMA-SOP0 observations.

### 5.2. Comparison of Model and Campaign Mean Observed Aerosol Profiles

[54] Figure 6 compares the model's vertical distribution of mineral dust and biomass burning aerosol, for the grid box closest to Niamey, with the DABEX campaign mean profiles from the FAAM aircraft (see section 4). Extinction profiles have been compared for wavelengths of 450, 550 and 700 nm, corresponding to the 3 channels of the nephelometer. The model and observations agreed reasonably well on the vertical profile and wavelength dependence of the extinction coefficient for both aerosol species. The agreement between model and observed aerosol profiles suggests that HadGEM2 performed reasonably well in its simulation of emission elevation (for biomass burning aerosol), vertical mixing, and large-scale transport in this region. The magnitude of aerosol extinction agreed well with the aircraft data because the AOD in the model was scaled to create agreement between observed and modeled AODs over the Niamey region (see previous section).

### 5.3. AODs and Radiative Effects Over West Africa

[55] Figures 7a and 7b show the modeled AOD of biomass burning aerosol and natural aerosols. The biomass burning AOD was very high (1–2) over central Africa. There was also a very rapid decrease in AOD with north-

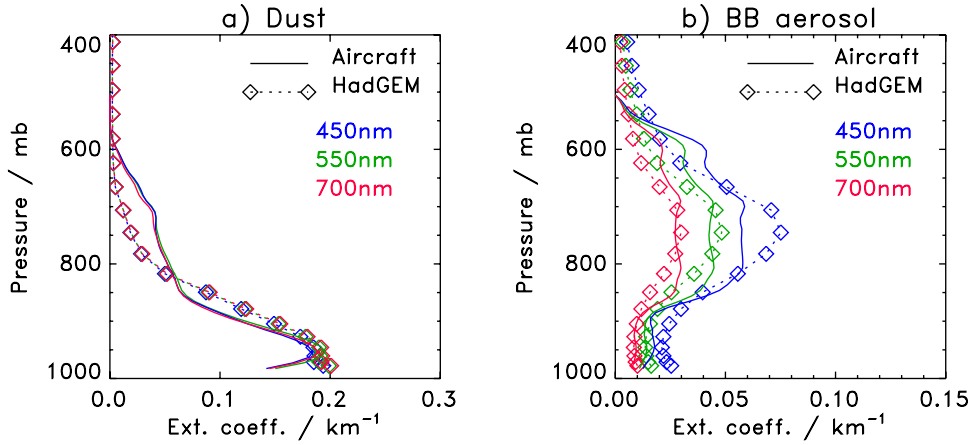


**Figure 6.** Comparison of HadGEM climate model (dotted lines with diamonds) and FAAM aircraft (solid lines) mean profiles of aerosol extinction at 450 nm, 550 nm, and 700 nm for (a) mineral dust and (b) biomass burning aerosol (solid) as a function of pressure.

ward distance across the Sahel. These features may indicate that there were excessive emissions over that region and too few emissions over the Sahel. This problem was also noted by Myhre et al. (submitted manuscript, 2008) and was linked to a high spot in the fuel load data from *Van der Werf et al.* [2006] used to calculate emission over Central Africa. Insufficient northward transport of aerosols over North Africa may also have contributed to the problem. The adjustment of AODs to create agreement between aircraft and model AODs over the Niamey region may have been partly responsible for the exaggerated AODs over central Africa and nearby ocean areas. The natural aerosol AOD was dominated by mineral dust from the Western Sahara. Sea salt and DMS-related sulphate were secondary contributors to the AOD, and were confined mainly to ocean areas. The natural aerosol AOD was between 0.2 and 0.5 over most

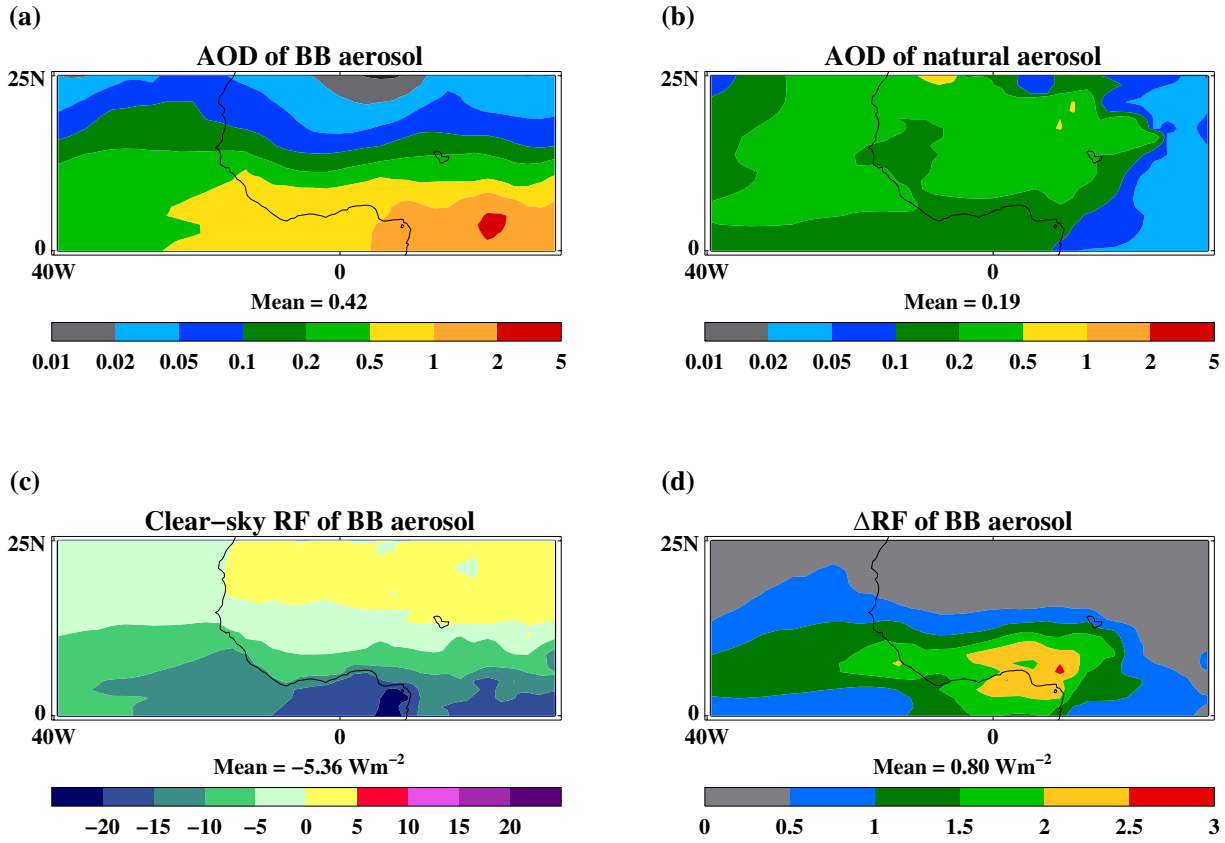


**Figure 7.** HadGEM January mean model output: (a) biomass burning AOD, (b) AOD of natural aerosols (dust, sea salt, and DMS-produced sulphate), (c) biomass burning aerosol radiative forcing at the top of the atmosphere, and (d) change in TOA radiative forcing of biomass burning aerosol when natural aerosols are considered as part of the background state.

of northwest Africa, which agrees well with satellite estimates [*Christopher et al.*, 2008].

[56] The clear-sky TOA radiative effect of biomass burning aerosol is shown in Figure 7c. Because of the low single scattering albedo (0.81 at 550 nm, see section 4.1.1) the radiative effect was positive over the bright surfaces of the Sahara desert. Over darker surfaces, such as ocean and vegetated land surfaces, the TOA radiative effect became negative. The largest negative effect was over the gulf of Guinea, where values exceed $-20$ W m$^{-2}$, because of the low surface albedo of ocean and high loading of biomass burning aerosols advected off central Africa (Figures 7a and 7c). The magnitude of the effect is likely to be too high here because of the overestimation of AOD. For the grid box over Niamey (13.3°N, 2.1°E) the biomass burning aerosol radiative effect was $-1.4$ W m$^{-2}$, which is very close to the value of $-1.3$ W m$^{-2}$ estimated from the single column calculations in section 4. The pattern of clear-sky TOA radiative effect is very similar to that obtained by Myhre et al. (submitted manuscript, 2008) using the OSLO-CTM2 chemical transport model with aerosol optical properties specified from the DABEX aircraft observations. They found the radiative effect of biomass burning aerosol changed from negative to positive at around 10°N across West Africa (a little further south than in Figure 7c), and attributed this to surface albedo variation.

[57] These TOA radiative effects were calculated in the absence of any natural aerosols. However, when natural aerosols were considered to be part of the background atmospheric state then the TOA radiative effect of the biomass burning increased by 1.5–3 W m$^{-2}$ over a broad part of the West African region (Figure 7d). This increase occurred because the natural aerosol (principally dust) was brightly reflective (single scattering albedo of 0.98 at 550 nm, see section 4.1.1) and increased the amount of scattered upwelling radiation. In this way, the dust layer had a similar effect as a small increase in surface albedo. The impact of natural aerosols on the TOA radiative effect of biomass burning ($\Delta$RF) aerosols was greatest in the southern Sahel and West African coastal region (Figure 7d) where there was a combination of high biomass burning AOD, high natural aerosol AOD, and low surface albedo. The change in radiative effect was 0.8 W m$^{-2}$ for the grid box over Niamey, and also 0.8 W m$^{-2}$ for the domain mean. These are not insignificant perturbations compared to domain mean radiative effect, which was $-5.4$ W m$^{-2}$.

[58] These results illustrate an interplay between absorbing and scattering aerosols at different altitudes. A more thorough assessment of biomass burning aerosol radiative effects in central and west African region would require longer integrations of the climate model, a more quantitative evaluation of the AOD fields against satellite and AERONET data, and an assessment of errors and uncertainties associated with emissions data, meridional transport of aerosol, and aerosol optical properties.

## 6. Summary and Discussion

[59] Measurements of aerosol extinction profile were made during DABEX/AMMA-SOP0 from a variety of platforms. These included in situ measurements by the FAAM aircraft, Raman and elastic backscatter lidar retrievals and micropulse lidar retrievals from ground sites, and lidar retrievals from an ultralight aircraft. The comparison tackled a complex situation where mixtures of fine and coarse aerosols from dessert dust and biomass burning were mixed together in varying proportions at different altitudes. Thick layers of mineral dust aerosol were found in the local boundary layer (up to about 2 km) and elevated layers of biomass burning aerosol, mixed to a variable degree with dust, were found at altitudes of 2–5 km. In general lidar and aircraft instruments performed well in capturing the variation of aerosol extinction with height. Absolute values of extinction coefficient sometimes differed between different instruments by up to a factor of 2. Such case-by-case differences may have been caused by differences of up to 100 km between the location of ground sites and aircraft profiles and by differences of 2 h or more in the timing measurements on some comparisons. However, by averaging data over a 3 week period from 13 January to 3 February, better agreement was generally found between lidars and aircraft in situ measurements.

[60] This study increases confidence in the ability of both lidars and aircraft in situ instruments (nephelometer and PSAP) to measure aerosol extinction as a function of altitude. The aircraft in situ measurements agreed well with AERONET AODs. However, uncertainties remain over the extent to which coarse particle might be lost during sampling by the FAAM aircraft. Uncertainties also remain in how to correct nephelometer data where a large proportion of the scattering is from coarse dust particles that are aspherical and have a strong forward scattering peak. The Raman technique gave reasonably accurate aerosol extinction coefficients as a function of altitude, and as a column mean. One difficultly of the Raman technique is that it relies on nighttime operation of the lidar and nighttime measurements were not available on every night. This led to extrapolation of lidar ratios across time periods of more than 24 h. Although extrapolation from night to day is unavoidable with Raman lidar, automated systems [e.g., *Ferrare et al.*, 2006] can improve data availability during day and night. The profile mean aerosol extinction from the micropulse lidar was constrained reasonably well by the AODs retrieved from the MFRSR, although some uncertainties were noted because of the shadow band of the MFRSR, which blocks diffuse radiation from small scattering angles. It is more difficult to correct for this when there is a large forward scattering peak due to large dust aerosol particles. The ULA techniques of horizontal shooting during ascents and descents proved to produce good results when compared with the POLIS ground-based or FAAM in situ measurements.

[61] The campaign mean profile of aerosol extinction coefficient from the FAAM aircraft was used to assess shortwave radiative effects of biomass burning aerosol and mineral dust aerosol over the Niamey region during DABEX/AMMA-SOP0. The change in net shortwave radiative flux at the top of the atmosphere, due to biomass burning aerosol was estimated to be about $-1.2$ W m$^{-2}$ in single-column radiative transfer calculations. This estimate was a small residual between a decrease of $-10.7$ W m$^{-2}$ in the net shortwave radiation at the surface and an increase of 9.5 W m$^{-2}$ in the absorption of shortwave radiation in the

atmosphere. The high level of absorption was a consequence of the moderate to high surface albedo (broadband value of 0.28) and the low single scattering albedo of the biomass burning aerosol (0.81 at 550 nm) estimated from the nephelometer and PSAP instruments on the FAAM aircraft. The TOA estimate is consistent with regional estimates of shortwave radiative effects from the Oslo CTM2 chemical transport model (Myhre et al., submitted manuscript, 2008). Uncertainties in these estimates of radiative effects stem largely from uncertainty in the estimated single scattering albedo, and uncertainty in estimating what proportion of the aerosol extinction was attributable to biomass burning emissions rather than mineral dust or other natural and anthropogenic emissions.

[62] The magnitudes of shortwave radiative effects were sensitive to the vertical distribution of aerosols. Single-column radiative transfer calculations showed a 1.8 W $m^{-2}$ increase in solar absorption due to the elevation of the biomass burning aerosol above the brightly reflective dust layer (the dust had a single scattering albedo of 0.98 at 550 nm). This response to scattering from below was not as strong as in cases from SAFARI-2000 where extensive decks of marine stratocumulus cloud were observed below elevated layers of biomass burning aerosol [*Keil and Haywood*, 2003; *Abel et al.*, 2005; *Myhre et al.*, 2003a]. However, given the current uncertainty in the sign of biomass burning aerosol radiative forcing at TOA, the sensitivities to vertical distribution shown in this study are still of interest. A similar level of sensitivity was also shown by *Meloni et al.* [2005] where different vertical distributions of moderately absorbing dust aerosol lead to changes of around 10% in clear-sky TOA radiative effects.

[63] The radiative interaction between mineral dust and biomass burning aerosol layers was also illustrated in climate model simulations with the HadGEM2-A model. HadGEM2-A performed well in simulating the observed vertical distributions of mineral dust and biomass burning aerosol over the Niamey region. The top of atmosphere radiative effect of the biomass burning aerosol was increased by 1.5–3 W $m^{-2}$, over a broad region of West Africa, when dust aerosol was included as part of the background state. However, the biomass burning AODs may have been too high in some parts of the model domain (especially central Africa) because of the adjustment of aerosol extinction to create agreement with the aircraft-derived optical depths over Niamey. Despite its limitations, the climate model experiment illustrates the need to consider the treatment of aerosol species in the assumed background state of the atmosphere when calculating radiative forcings of anthropogenic absorbing aerosols. The vertical interactions between shortwave radiation and aerosol, implied by this study, also raise interesting questions about how the vertical distribution of aerosol might affect remote sensing retrievals of aerosol column properties from both the ground and space.

[64] **Acknowledgments.** The FAAM aircraft is jointly funded by the Met Office and the Natural Environment Research Council. The work of B.H. was funded by the African Monsoon Multidisciplinary Analysis (AMMA) (http://www.amma-international.org). The AMF data were provided by the U.S. Department of Energy as part of the Atmospheric Radiation Measurement Program Climate Research Facility. The authors thank Connor Flynn for help processing the MPL data. The contributions of A. J. and N. B. were supported by the UK Department for the Environment, Food and Rural Affairs and Ministry of Defence Integrated Climate Programme–GA01101, CBC/2B/0417-Annex C5. P. C. was funded by Centre National d'Etudes Spatiales (CNES) and by Commissariat á l'Energie Atomique (CEA). We also thank Didier Tanŕe for his efforts in establishing and maintaining the Banizoumbou AERONET site.

## References

Abel, S. J., E. J. Highwood, J. M. Haywood, and M. A. Stringer (2005), The direct radiative effect of biomass burning aerosols over southern Africa, *Atmos. Chem. Phys.*, *5*, 1999–2018.

Ackerman, S., O. B. Toon, D. E. Stevens, A. J. Heymsfield, V. Ramanathan, and E. J. Welton (2000), Reduction of tropical cloudiness, *Science*, *288*, 1042–1047.

Alexandrov, M. D., P. Kiedron, J. J. Michalsky, G. Hodges, C. J. Flynn, and A. A. Lacis (2007), Optical depth measurements by shadow-band radiometers and their uncertainties, *Appl. Opt.*, *46*, 8027–8038.

Anderson, T. L., and J. A. Ogren (1998), Determining aerosol radiative properties using the TSI 3563 integrating nephelometer, *Aerosol Sci. Technol.*, *29*, 57–69.

Andres, R. J., and A. D. Kasgnoc (1998), A time-averaged inventory of subaerial volcanic sulfur emissions, *J. Geophys. Res.*, *103*, 25,251–25,261, doi:10.1029/98JD02091.

Ansmann, A., U. Wandinger, M. Riebesell, C. Weitkamp, and W. Michaelis (1992), Independent measurement of extinction and backscatter profiles in cirrus clouds by using a combined Raman elastic-backscatter lidar, *Appl. Opt.*, *31*(33), 7113–7131.

Bellouin, N., O. Boucher, J. M. Haywood, C. E. Johnson, A. Jones, J. G. L. Rae, and S. Woodward (2007), Improved representation of aerosols for HadGEM2, *Tech. Note 73*, Hadley Cent., Exeter, U. K. (Available at http://www.metoffice.gov.uk/research/hadleycentre/pubs/HCTN/index.html)

Campbell, J. R., D. L. Hlavka, E. J. Welton, C. J. Flynn, D. D. Turner, J. D. Spinhirne, V. S. Scott, and I. H. Hwange (2002), Full-time eye-safe cloud and aerosol lidar observation at Atmospheric Radiation Measurement Program sites: Instruments and data processing, *J. Atmos. Oceanic Technol.*, *19*(4), 431–442.

Capes, G., B. T. Johnson, G. McFiggans, P. I. Williams, J. M. Haywood, and H. Coe (2008), Aging of biomass burning aerosols over West Africa: Aircraft measurements of chemical composition, microphysical properties and emission ratios, *J. Geophys. Res.*, doi:10.1029/2008JD009845, in press.

Chazette, P., J. Sanak, and F. Dulac (2007), New approach for aerosol profiling with a lidar onboard an ultra light aircraft: Application to the African Monsoon Multidisciplinary Analysis, *Environ. Sci. Technol.*, *41*, 8335–8341.

Christopher, S. A., P. Gupta, J. Haywood, and G. Greed (2008), Aerosol optical thicknesses over North Africa: 1. Development of a product for model validation using Ozone Monitoring Instrument, Multiangle Imaging Spectroradiometer, and Aerosol Robotic Network, *J. Geophys. Res.*, *113*, D00C04, doi:10.1029/2007JD009446.

Cox, C., and W. Munk (1954), Statistics of the sea surface derived from sun glitter, *J. Mar. Res.*, *13*, 198–227.

Davison, P. S., D. L. Roberts, R. T. Arnold, and R. N. Colville (2004), Estimating the direct radiative forcing due to haze from the 1997 forest fires in Indonesia, *J. Geophys. Res.*, *109*, D10207, doi:10.1029/2003JD004264.

Dentener, F., et al. (2006), Emissions of primary aerosol and precursor gases in the years 2000 and 1750 prescribed data-sets for AeroCom, *Atmos. Chem. Phys.*, *6*, 4321–4344.

Edwards, J. M., and A. S. Slingo (1996), Studies with a flexible radiation code. I: Choosing a configuration for a large-scale model, *Q. J. R. Meteorol. Soc.*, *122*, 689–719.

Fernald, F. G. (1984), Analysis of atmospheric lidar observations, *Appl. Opt.*, *23*, 652–653.

Ferrare, R. A., et al. (2006), Evaluation of daytime measurements of aerosols and water vapor made by an operational Raman lidar over the Southern Great Plains, *J. Geophys. Res.*, *111*, D05S08, doi:10.1029/2005JD005836.

Formenti, P., et al. (2008), Composition of mineral dust from western Africa: Results from the AMMA SOP0/DABEX and DODO field campaigns, *J. Geophys. Res.*, doi:10.1029/2008JD009903, in press.

Forster, P., et al. (2007), Changes in atmospheric constituents and in radiative forcing, in *Climate Change 2007: The Physical Science Basis—Contribution of Working Group I to the Fourth Assessment Report of the Intergovernmental Panel on Climate Change*, edited by S. Solomon et al., pp. 129–234, Cambridge Univ. Press, Cambridge, U. K.

Gadhavi, H., and A. Jayaraman (2006), Airborne lidar study of the vertical distribution of aerosol over Hyderabad, an urban site in central India, and its implication for radiative forcing calculations, *Ann. Geophys.*, *24*(10), 2461–2470.

Ginoux, P., and O. Torres (2003), Empirical TOMS index for dust aerosol: Applications to model validation and source characterization, *J. Geophys. Res.*, *108*(D17), 4534, doi:10.1029/2003JD003470.

Harrison, L., and J. Michalsky (1994), Objective algorithms for the retrieval of optical depths from ground-based measurements, *Appl. Opt.*, *33*(22), 5126–5132.

Haywood, J. M., and V. Ramaswamy (1998), Global sensitivity studies of the direct radiative forcing due to anthropogenic sulfate and black carbon aerosols, *J. Geophys. Res.*, *103*(D6), 6043–6058.

Haywood, J. M., P. Francis, S. R. Osborne, M. Glew, N. Leob, E. Highwood, D. Tanŕe, G. Myhre, P. Formenti, and E. Hirst (2003a), Radiative properties and direct radiative effect of Saharan dust measured by the C-130 aircraft during SHADE: 1. Solar spectrum, *J. Geophys. Res.*, *108*(D18), 8577, doi:10.1029/2002JD002687.

Haywood, J. M., P. Francis, O. Dubovik, M. Glew, and B. Holben (2003b), Comparison of aerosol size distributions radiative properties and optical depths determined by aircraft observations and Sun photometers during SAFARI 2000, *J. Geophys. Res.*, *108*(D13), 8471, doi:10.1029/2002JD002250.

Haywood, J. M., S. R. Osborne, and S. J. Abel (2004), The effect of overlying absorbing aerosol layers on remote sensing retrievals of cloud effective radius and cloud optical depth, *Q. J. R. Meteorol. Soc.*, *130*, 779–800.

Heese, B., and M. Wiegner (2008), Vertical aerosol profiles from Raman-depolarization lidar observations during the dry season AMMA field campaign, *J. Geophys. Res.*, *113*, D00C11, doi:10.1029/2007JD009487.

Heese, B., V. Freudenthaler, M. Seefeldner, and M. Wiegner (2002), POLIS—A new Portable Lidar System for ground-based and airborne measurements of aerosols and clouds, paper presented at International Laser Radar Conference, Def. R&D Can.–Valcartier, Quebec City, Que., Canada, July.

Heese, B., V. Freudenthaler, M. Seefeldner, M. Kosmale, and M. Wiegner (2004), First results from the portable lidar system POLIS, in *Proceedings of the International Laser Radar Conference*, *Eur. Space Agency Spec. Publ.*, *ESA SP-561*, 79–92.

Hsu, N. C., J. R. Herman, and S. C. Tsay (2003), Radiative impacts from biomass burning in the presence of clouds during boreal spring in southeast Asia, *Geophys. Res. Lett.*, *30*(5), 1224, doi:10.1029/2002GL016485.

Johns, T. C., et al. (2006), The new Hadley Centre climate model (HadGEM1): Evaluation of coupled simulations, *J. Clim.*, *19*, 1327–1353, doi:10.1175/JCLI3712.1.

Johnson, B. T., K. P. Shine, and P. M. Forster (2004), The semi-direct aerosol effect: Impact of absorbing aerosols on marine stratocumulus, *Q. J. R. Meteorol. Soc.*, *130*, 1407–1422.

Johnson, B. J., J. Pelon, P. Formenti, and J. Haywood (2007), Aerosol studies during AMMA, *Clivar Exch.*, *12*(2), 9–11.

Johnson, B. T., S. R. Osborne, and J. M. Haywood (2008), Aircraft measurements of biomass burning aerosol over West Africa during DABEX, *J. Geophys. Res.*, *113*, D00C06, doi:10.1029/2007JD009451.

Jones, A., D. L. Roberts, M. J. Woodage, and C. E. Johnson (2001), Indirect sulphate aerosol forcing in a climate model with an interactive sulphur cycle, *J. Geophys. Res.*, *106*, 20,293–20,310, doi:10.1029/2000JD000089.

Keil, A., and J. M. Haywood (2003), Solar radiative forcing by biomass burning aerosol particles during SAFARI 2000: A case study based on measured aerosol and cloud properties, *J. Geophys. Res.*, *108*(D13), 8467, doi:10.1029/2002JD002315.

Kettle, A. J., et al. (1999), A global database of sea-surface dimethylsulfide (DMS) measurements and a procedure to predict sea surface DMS as a function of latitude, longitude and month, *Global Biogeochem. Cycles*, *13*, 399–444.

Klett, J. D. (1985), Lidar inversion with variable backscatter/extinction ratios, *Appl. Opt.*, *24*(11), 833–835.

Léon, J. F., P. Chazette, J. Pelon, F. Dulac, and H. Randriamiarisoa (2002), Aerosol direct radiative impact over the INDOEX area based on passive and active remote sensing, *J. Geophys. Res.*, *107*(D19), 8006, doi:10.1029/2000JD000116.

Mallet, M., et al. (2008), Aerosol direct radiative forcing over Djougou (northern Benin) during the African Monsoon Multidisciplinary Analysis dry season experiment (Special Observation Period-0), *J. Geophys. Res.*, *113*, D00C01, doi:10.1029/2007JD009419.

Martin, G. M., M. A. Ringer, V. D. Pope, A. Jones, C. Dearden, and T. J. Hinton (2006), The physical properties of the atmosphere in the new Hadley Centre Global Environment Model (HadGEM1). Part I: Model description and global climatology, *J. Clim.*, *19*, 1274–1301, doi:10.1175/JCLI3636.1.

Masonis, S. J., K. Franke, A. Ansmann, D. Muller, D. Althausen, J. A. Ogren, A. Jefferson, and P. J. Sheridan (2002), An intercomparison of aerosol light extinction and 180°-backscatter as derived using in situ instruments and Raman lidar during the INDOEX campaign, *J. Geophys. Res.*, *107*(D19), 8014, doi:10.1029/2000JD000035.

McClatchey, R. A., R. W. Fenn, J. E. A. Selby, F. E. Volz, and J. S. Garing (1972), Optical properties of the atmosphere, 3rd ed., *Rep. AFCRL-72-0497*, Air Force Cambridge Res. Lab., Hanscom Air Force Base, Mass.

McConnell, C. L., E. J. Highwood, H. Coe, P. Formenti, B. Anderson, S. Osborne, S. Nava, K. Desboeufs, G. Chen, and M. A. J. Harrison (2008), Seasonal variations of the physical and optical characteristics of Saharan dust: Results from the Dust Outflow and Deposition to the Ocean (DODO) experiment, *J. Geophys. Res.*, *113*, D14S05, doi:10.1029/2007JD009606.

McFarquhar, G. M., and H. L. Wang (2006), Effects of aerosols on trade wind cumuli over the Indian Ocean: Model simulations, *Q. J. R. Meteorol. Soc.*, *132*, 821–843.

Meloni, D., A. di Sarra, T. Di Iorio, and G. Fiocco (2005), Influence of the vertical profile of Saharan dust on the visible direct radiative forcing, *J. Quant. Spectrosc. Radiat. Transfer*, *93*, 397–413.

Miller, M. A., and A. Slingo (2007), The Atmospheric Radiation Measurement (ARM) Mobile Facility (AMF) and its first international deployment: Measuring radiative flux divergence in West Africa, *Bull. Am. Meteorol. Soc.*, *88*(8), 1229–1244.

Myhre, G., T. Berntsen, J. M. Haywood, J. K. Sundet, B. N. Holben, M. Johnsrud, and F. Stordal (2003a), Modelling the solar radiative impact of aerosol from biomass burning during the Southern African Regional Science Initiative (SAFARI-2000) experiment, *J. Geophys. Res.*, *108*(D13), 8501, doi:10.1029/2002JD002313.

Myhre, G., A. Grini, J. M. Haywood, F. Stordal, B. Chatenet, D. Tanŕe, J. K. Sundet, and I. S. A. Isaksen (2003b), Modelling the radiavtive impact of mineral dust during the Saharan Dust Experiment (SHADE) campaign, *J. Geophys. Res.*, *108*(D18), 8579, doi:10.1029/2002JD002566.

Osborne, S. R., J. M. Haywood, and N. Bellouin (2007), In situ and remote-sensing measurements of the mean microphysical and optical properties of industrial pollution aerosol during ADRIEX, *Q. J. R. Meteorol. Soc.*, *133*(S1), 17–32.

Osborne, S. R., B. T. Johnson, J. M. Haywood, A. J. Baran, M. A. J. Harrison, and C. L. McConnell (2008), Physical and optical properties of mineral dust aerosol during the Dust and Biomass-burning Experiment, *J. Geophys. Res.*, *113*, D00C03, doi:10.1029/2007JD009551.

Pal, S., W. Steinbrecht, and A. Carswell (1992), Automated method for lidar determination of cloud-base and vertical extent, *Appl. Opt.*, *31*, 1488–1494.

Quijano, A. L., I. N. Sokolik, and O. B. Toon (2000), Radiative heating rates and direct radiative forcing by mineral dust in cloudy atmospheric conditions, *J. Geophys. Res.*, *105*, 12,207–12,219.

Rajot, J. L., et al. (2008), AMMA dust experiment: An overview of measurements performed during the dry season special observation period (SOP0) at the Banizoumbou (Niger) supersite, *J. Geophys. Res.*, doi:10.1029/2008JD009906, in press.

Ramanathan, V., M. V. Ramana, G. Roberts, D. Kim, C. Corrigan, C. Chung, and D. Winker (2007), Warming trends in Asia amplified by brown cloud solar absorption, *Nature*, *448*, 575–578, doi:10.1038/nature06019.

Ross, J. L., and P. V. Hobbs (1998), Radiative characteristics of regional hazes dominated by smoke from biomass burning in Brazil: Closure tests and direct radiative forcing, *J. Geophys. Res.*, *103*(D24), 31,925–31,941.

Russell, P. B., J. M. Livingston, O. Dubovik, S. A. Ramirez, J. Wang, J. Redemann, B. Schmid, M. Box, and B. N. Holben (2004), Sunlight transmission through desert dust and marine aerosols: Diffuse light corrections to Sun photometry and pyrheliometry, *J. Geophys. Res.*, *109*, D08207, doi:10.1029/2003JD004292.

Schmid, B., J. Michalsky, R. Halthore, M. Beauharnois, L. Harrison, J. Livingston, P. Russell, B. Holben, T. Eck, and A. Smirnov (1999), Comparison of Aerosol Optical Depth from Four Solar Radiometers during the Fall 1997 ARM Intensive Observation Period, *Geophys. Res. Lett.*, *26*(17), 2725–2728.

Schmid, B., et al. (2006), How well do state-of-the-art techniques measureing the vertical profile of tropospheric aerosol extinction compare?, *J. Geophys. Res.*, *111*, D05S07, doi:10.1029/2005JD005837.

Tanŕe, D., J. Haywood, J. Pelon, J. F. Leon, B. Chatenet, P. Formenti, P. Francis, P. Goloub, E. J. Highwood, and G. Myhre (2003), Measurement and modelling of the Saharan dust radiative impact: Overview of the Saharan Dust Experiment (SHADE), *J. Geophys. Res.*, *108*(D18), 8574, doi:10.1029/2002JD003273.

Van der Werf, G. R., et al. (2006), Interannual variability in global biomass burning emissions from 1997 to 2004, *Atmos. Chem. Phys.*, *6*, 3423–3441.

Welton, E. J., and J. R. Campbell (2002), Micropulse lidar signals: Uncertainty analysis, *J. Atmos. Oceanic Technol.*, *19*, 2089–2094.

Welton, E. J., et al. (2000), Ground-based lidar measurements of aerosols during ACE-2: Instrument description, results, and comparisons with other ground-based and airborne measurements, *Tellus, Ser. B*, *52*(2), 636–651.

Won, J.-G., S.-C. Yoon, S.-W. Kim, A. Jefferson, E. G. Dutton, and B. Holben (2004), Estimation of direct radiative forcing of Asian dust aerosols with Sun/sky radiometer and lidar measurements at Gosan, Korea, *J. Meteorol. Soc. Jpn.*, *82*, 115–130.

Woodward, S. (2001), Modelling the atmospheric life-cycle and radiative impact of mineral dust in the Hadley Centre climate model, *J. Geophys. Res.*, *106*, 18,155–18,166, doi:10.1029/2000JD900795.

World Climate Program (1986), A preliminary cloudless standard atmosphere for radiation computation, World Meteorol. Organ., Geneva, Switzerland.

N. Bellouin, B. T. Johnson, and A. Jones, Met Office, Fitzroy Road, Exeter EX1 3PB, UK. (ben.johnson@metoffice.gov.uk)

P. Chazette, Laboratoire des Sciences du Climat et de l'Environnement, UVSQ, CEA Saclay, CNRS, F-91191 Gif-sur-Yvette, France.

B. Heese, Leibniz Institute for Tropospheric Research, D-04318 Leipzig, Germany.

S. A. McFarlane, Pacific Northwest National Laboratory, Richland, WA 99352, USA.